Journal of Cluster Science (2019) 30:459–468
https://doi.org/10.1007/s10876-019-01508-9

ORIGINAL PAPER

Catalytic Degradation of Methyl Orange and Selective Sensing of Mercury Ion in Aqueous Solutions Using Green Synthesized Silver Nanoparticles from the Seeds of *Derris trifoliata*

Neethu Cyril[1,2] · James Baben George[3] · Laigi Joseph[1,4] · V. P. Sylas[1]

Received: 20 November 2018 / Published online: 28 January 2019

Abstract
In the present study, bio-augmented silver nanoparticles with *Derris trifoliata* seed extract (AgNP-DT) have been developed. Formation of AgNP-DT has been confirmed with X-ray diffraction (XRD), High resolution transmission electron microscopy (HRTEM) and Fourier-transform infrared spectroscopy (FTIR). Even though introduced for the first time as a catalyst owing to high surface area, the as-prepared nanoparticles showed one of the best catalytic activity in the reduction of a water soluble azo dye–methyl orange. An incredible pseudo-first order rate constant (0.3208 min^{-1}) and activity parameter (1086 s^{-1} g^{-1}) were obtained for the catalytic reduction of methyl orange with 4.9 μg AgNP-DT. Furthermore, AgNP-DT exhibits a good selectivity and sensitivity towards mercury(II) ions over other metals in aqueous solution. Absorbance of AgNP-DT exhibits a good linear relationship against concentration of Hg^{2+} with a limit of detection (LOD) of 1.55 μM. The mechanism of sensing activity of AgNP-DT was elucidated by measuring the variation in the zeta potential of the system with increasing concentration of Hg^{2+}. Moreover the proposed method could be practicably applied for the detection of Hg^{2+} in real water samples with a percentage recovery in range of 91.41–108.07%.

✉ V. P. Sylas
sylas@mgu.ac.in; mgubioenergy@gmail.com

[1] School of Environmental Sciences, Mahatma Gandhi University, Kottayam, Kerala 686 560, India

[2] Department of Chemistry, Assumption College, Changanasserry, Kottayam, Kerala 686 101, India

[3] Department of Chemistry, St. Berchman's College, Changanasserry, Kottayam, Kerala 686 101, India

[4] Department of Chemistry, Government College, Nattakom, Kottayam, Kerala 686 013, India

Graphical Abstract

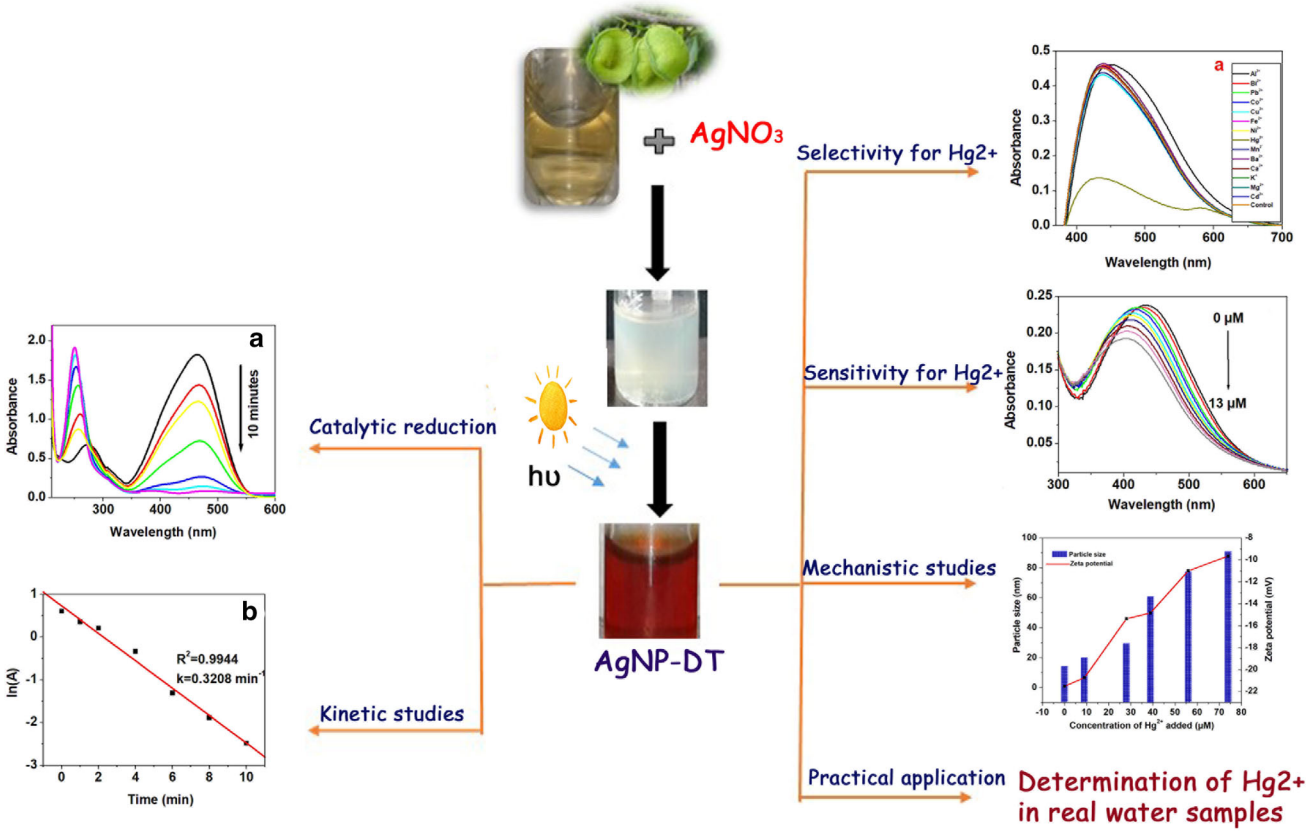

Keywords Silver nanoparticles · *Derris trifoliata* · Catalytic activity · Mercury ion · Activity parameter

Introduction

Heavy metals and artificial dyes causes many serious problems to human and environment [1]. Usage of these chemicals are unavoidable for their wide applications in different fields of science and technology. With rapid development of industries such as textile industry, ore mining, paint and paper industry, pesticide and fertilizer industry etc., a huge amount of dyes, pigments and heavy metals are disposed after the industrial processes. The effluents from these industries are discharged into natural surface and ground water resources. These pollutants alters the chemistry of surface water and thus affects the health of living organisms. With passage of time, dyes and pigments present in water undergoes chemical degradation or transformation to form more toxic products. Heavy metals and dyes could directly or indirectly enter the food chain and cause severe toxic impacts on the environment. Therefore, it is critical to detect and reduce or remove these industrial pollutants from water.

There are several techniques reported in the literature for the treatment of dye contaminated waste water. These include catalytic reduction [2], photocatalytic degradation [3], advanced oxidation processes [4], membrane techniques [5], bioremediation [6] and adsorption [7, 8]. Among them, reductive degradation using nanocatalyst have been applied widely for the treatment of dyes in aqueous solutions due to its low cost, clean processing and efficiency [9, 10]. Reduction of dyes with nanocatalyst convert them to readily biodegradable products which can be further treated if required [10]. Metal based nanocatalysts for the reduction reaction mainly rely on noble metals, such as Au and Ag

[11, 12] due to their high stability and large surface area. However, without suitable surface stabilizers, these nanocatalysts undergo aggregation, which can lead to degradation of their catalytic activities and lifetime [13]. Therefore, it is important to stabilize nanocatalyst with proper ligands to improve its lifetime and efficiency. Recently, bio-augmented metal nanocatalysts have been prepared by utilizing different parts of plants, algae, micro-organisms and enzymes [14]. Due to its highly stable and dispersive nature in water, these bio-functionalised nanocatalysts could be effectively applied for catalysing the reduction reaction of water soluble dyes [15].

Among heavy metals, mercury is one of the highly toxic pollutants in aquatic environments [16]. Inorganic salts of mercury are highly water soluble and thus Hg^{2+} exists mostly in surface waters. Mercury binds with sulfhydryl groups of enzymes and amino acids and induces mitochondrial dysfunction with subsequent increase in oxidative stress causing hypertension, cardiovascular disease, stroke etc. [17]. There are several methods reported for the selective mercury detection like atomic fluorescence spectrometry (AFS), atomic absorption/emission spectrometry (AAS/AES), inductively coupled plasma mass spectrometry (ICPMS) etc. [18]. However these methods are expensive and require laborious sample preparation and pre-concentration procedures. Hence, the interest in cost-effective analytical methods with selective and sensitive mercury(II) ion sensors have been increasing. Various sensor systems for the detection of mercury(II), based on polymers [19], organic compounds [20], functionalised nanoparticles [21], carbon dots [22], DNA [23] and chromophores [24] have been reported. Nowadays metal nanoparticles and their composites are widely applied for the sensing of organic and inorganic molecules like alcohols [25], thiols [26], 2,4-dinitrotoluene [27], glutathione [28], hydrogen peroxide [29, 30], heavy metals [31, 32] and even rare earth metals [33]. Among them, mercury sensors based on bio-functionalised metal nanoparticles have been extremely attended due to their simplicity, selectivity and ease of measurement. Farhadi et al. have developed a mercuric colorimetric sensor of silver nanoparticles stabilized with soap-root plant extract which could detect Hg^{2+} in micromolar level [21]. Unlike other metal nanoparticles, silver nanoparticles are stable for several months, allowing these nanoparticles to be utilized for sensitive detection with minimum consumption of materials [34].

Derris trifoliata belongs to the family Leguminosae, is an underutilised mangrove associated plant species commonly seen in tropical region. Very few studies were reported on the chemical and medicinal applications of *Derris trifoliata*. Catalytic activity and metal sensing ability of nanoparticles capped with *Derris trifoliata* extract have not yet been evaluated. Therefore the present study focus on the catalytic potential of AgNP-DT for the reductive degradation of an azo dye, methyl orange. Also the metal sensing ability of AgNP-DT was explored for the selective sensing of Hg^{2+} ions from water samples.

Materials and Methods

Seeds of *Derris trifoliata* were collected from Vembanad-Kol Ramsar site, Kerala, India. Methyl orange, Sodium borohydride ($NaBH_4$), Silver nitrate ($AgNO_3$) and mercuric chloride were procured from Merck India Ltd. and used without further purification. All aqueous solutions were prepared using double distilled water.

Synthesis and Characterisation of AgNP-DT

10 g of seed powder was extracted with 50 mL of distilled water for 30 min and filtered. The presence of phytochemical constituents in the aqueous seed extract was analysed by standard preliminary phytochemical tests [35, 36]. 250 µL of seed extract was then added to 5 mL of 1 mM solution of $AgNO_3$ and kept under sunlight. The above experiment was repeated at room temperature under the same experimental conditions in the absence of sunlight. The silver nanoparticles synthesized by the assistance of sunlight were characterized by spectroscopic and microscopic techniques. UV–visible studies were carried out using Shimadzu UV-1700 Pharmaspec spectrophotometer. The IR spectra have been recorded using Shimadzu IR Prestige-21 FTIR spectrometer. X-ray diffraction (XRD) analysis were performed by Mini Flex 600-Rigaku diffractometer. The size and morphology of nanoparticles were examined by high resolution transmission electron microscope (HRTEM). DLS measurements were carried out by Litesizer^{TM} 500 Anton Paar GmbH analyser.

Catalytic Reduction of Methyl Orange (MO)

The reduction of methyl orange with $NaBH_4$ was used to study the catalytic efficacy of AgNP-DT. To 50 µL of 5 mM methyl orange taken in the quartz cuvette, 0.1 mL of 0.5% w/v freshly prepared $NaBH_4$ solution was added. It was followed by the addition of 30 µL of AgNP-DT and the solution was made up to 3.2 mL with distilled water. The variation in the concentration of methyl orange was observed using UV–visible spectroscopy.

Colorimetric Detection of Mercury(II) Ion in the Aqueous Solution Using AgNP-DT

For the colorimetric detection of Hg^{2+}, the prepared AgNP-DT was diluted twenty times with double distilled

water. To examine the metal ion detection ability of AgNP-DT, representative alkali metals, alkaline earth metals and transition metal ions at same concentration (500 µL, 10^{-4} M) were added into 2 mL of diluted AgNP-DT at room temperature. The photographs were taken after 5 min of mixing and the change in the surface plasmon resonance (SPR) of AgNP-DT was monitored by UV–visible spectroscopy. Further, we employed the proposed sensing method for the determination of spiked concentration of Hg^{2+} in a river water (environmental matrix) collected from Meenachil River, Kerala, India and tap water collected from School of Environmental Sciences, MG University campus. The minimum detectable limit of Hg^{2+} in aqueous solution was also investigated.

Results and Discussion

Formation and Characterisation of AgNP-DT

Upon sunlight irradiation, colour of the reaction medium changes to yellowish dark-brown (Fig. 2a, b) indicating the formation of AgNP-DT. Figure 1a shows the UV–Vis spectrum of AgNP-DT formed at 15 min and 1 h of sunlight irradiation. The surface plasmon resonance (SPR) of AgNP-DT experienced a blue shift from 435 to 419 nm with increase in the time of irradiation and almost completes within 2 h. This may be due to the decrease in the size of nanoparticle with increase in duration of sunlight irradiation. For synthesizing AgNP-DT for catalytic reduction reaction of MO, the reaction mixture was kept under sunlight for 1 h, till the SPR peak reaches a wavelength of 419 nm. However, mercury sensing was effective even with AgNP-DT with SPR peak at 435 nm, formed upon an irradiation time of 15 min without any variation in its sensitivity. XRD measurements (Fig. 1b) showed diffraction peaks at 2θ values of 38.12°, 44.41°, 64.70° and 77.40°. These XRD peaks are compared with JCPDS number 87 - 0720 and it corresponds to (111), (200), (220) and (311) planes of a face centred cubic structures of silver crystals [37]. The average size of AgNP-DT (D) was calculated to be 16.05 ± 5.0 nm using Debye–Scherrer equation,

$$Particlesize(D) = \frac{k \times \lambda}{\beta \times \mathrm{Cos}\theta}$$

where k is Scherrer constant (0.9 for spherical crystals), λ is wavelength of X-ray, β is full width at half maximum (FWHM) and θ is the diffraction angle [38].

TEM images (Fig. 2c) revealed nearly spherical shape of AgNP-DT with $d_{(111)}$ spacing values measured to be 0.23 nm. The crystal planes of AgNP-DT and selected area electron diffraction patterns (SAED) of AgNP-DT corresponding to their Bragg's reflections were clearly shown in Fig. 2c.

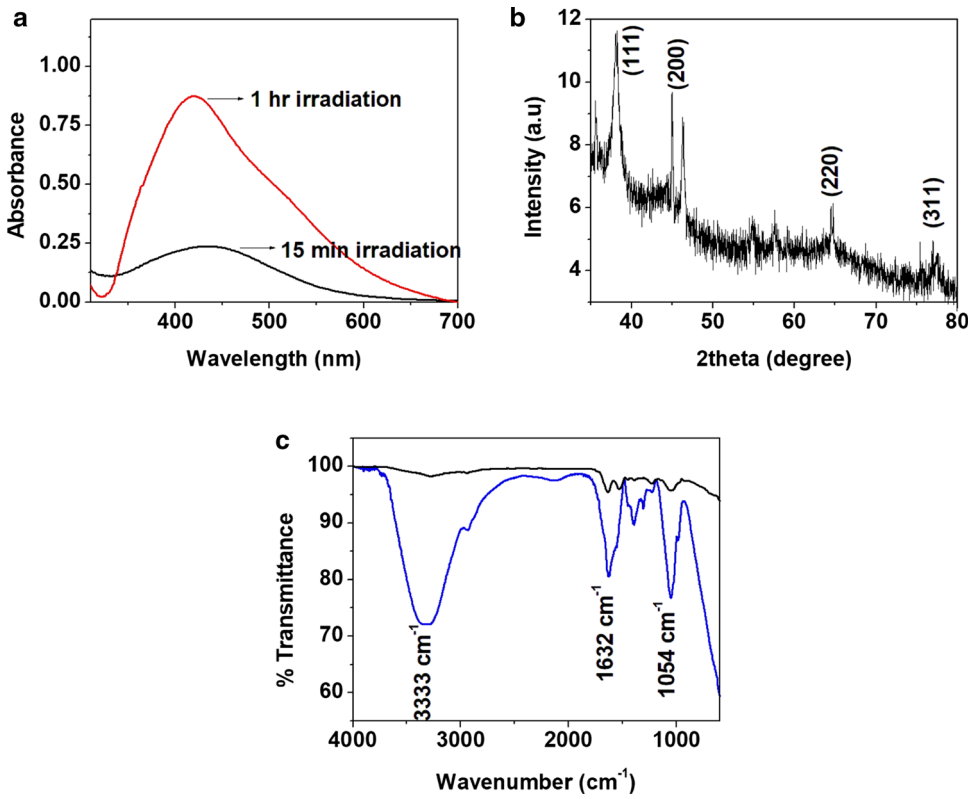

Fig. 1 **a** UV–vis spectra of AgNP-DT, **b** XRD pattern of AgNP-DT and **c** FTIR spectra of seed extract of *Derris trifoliata* and AGNP-DT

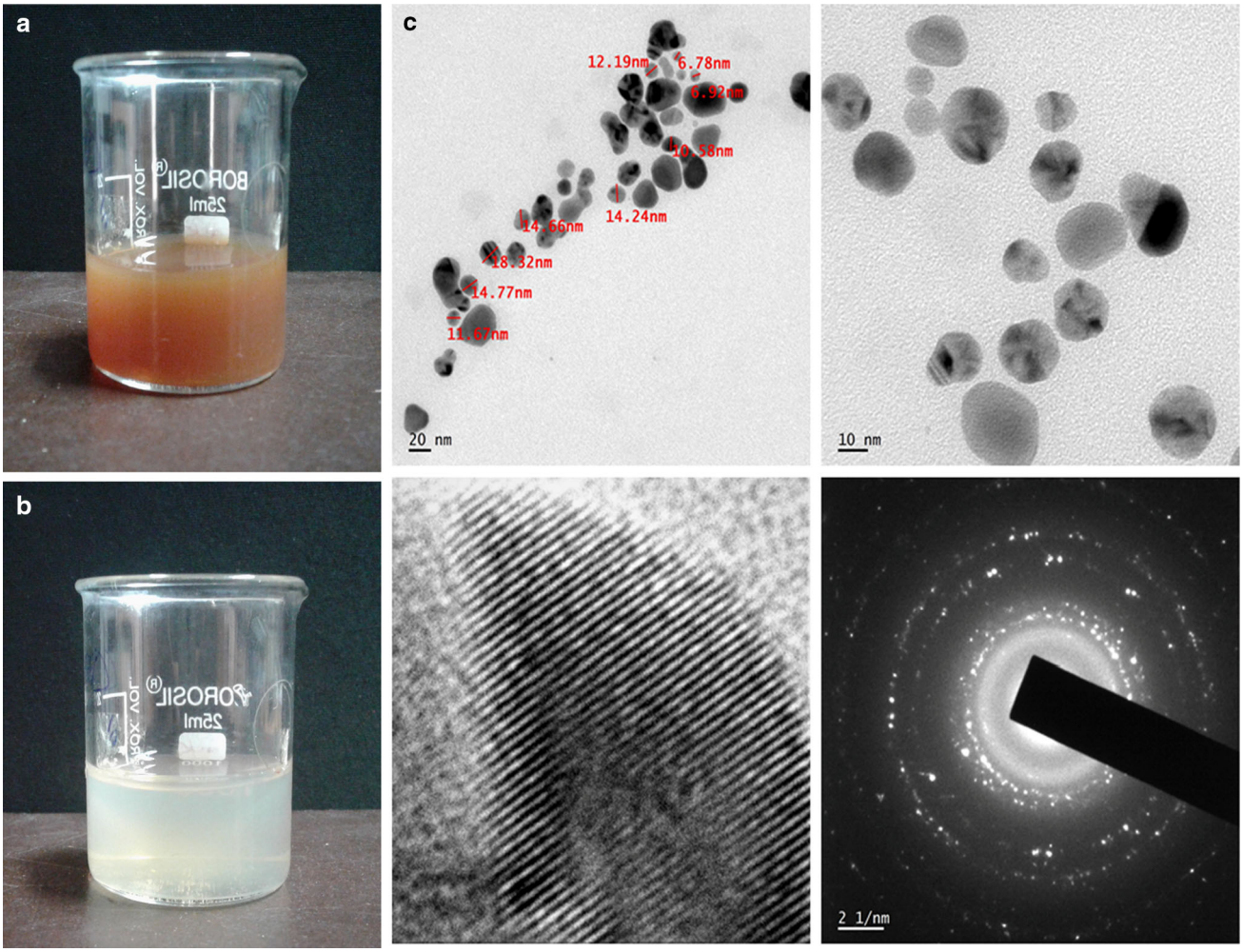

Fig. 2 **a** *Derris trifoliata* seed extract in $AgNO_3$ before sunlight irradiation, **b** AgNP-DT formed after sunlight irradiation and **c** HRTEM images of AGNP-DT

Derris trifoliata is already reported to contain bioactive compounds like flavonoids [39], isoflavonoids [40], phenolic acids [41] and polysaccharides [42]. Qualitative phytochemical analysis of the aqueous seed extract of *Derris trifoliata* confirm the presence of secondary metabolites like polyphenols, proteins, flavonoids and alkaloids. Figure 1c shows the FTIR spectra of *Derris trifoliata* and AgNP-DT nanoparticles. A broad and strong peak at 3333 cm^{-1} could be attributed to the –OH stretching vibrations of polyphenolic compounds [43]. The weak band at 2938 cm^{-1} could be assigned to the aliphatic C–H stretching and a peak at 1402 cm^{-1} correspond to geminal methyl of secondary metabolites in the aqueous extract [44]. The band at 1632 cm^{-1} was assigned to carbonyl (C=O) stretching in carboxyl group (amide I band) of proteins [45]. The band at 1054 cm^{-1} correspond to CN^{-} stretching of amines [46]. Comparing the FTIR spectrum of *Derris trifoliata* with that of AgNP-DT, the peaks at 1632 cm^{-1} and 1054 cm^{-1} were the prominent ones present in both the spectra. These peaks correspond to the carbonyl and amine groups which might be responsible for the capping of silver nanoparticles. These capping ligands itself could act as reducing and stabilizing agents. The nitrogen or oxygen atom of the capping agent could donate lone pairs of electrons to Ag^{+} ions for its reduction to Ag^{0}. This reaction proceed at a very slow in the absence of sunlight. At room temperature, it takes minimum 48 h for the formation of AgNP-DT. In the presence of sunlight, the capping agent could easily donate electrons for the reduction of silver ions. This confirms the catalytic behaviour of sunlight in the formation of AgNP-DT.

Catalytic Reduction of Methyl Orange (MO)

Methyl orange is an azo dye which is widely used as pH indicator as well as for dyeing of fabrics. The catalytic reduction of MO was studied using synthesized AgNP-DT in the presence of excess $NaBH_4$. The reduction of MO with

$NaBH_4$, in the absence of a catalyst occurs at a very slow rate (Fig. 4c). This may be due to the presence of high energy barrier between the mutually repelling negative ions of borohydride (BH_4^-) and methyl orange. In the present work, 30 µL of AgNP-DT was used for the reduction of MO. 30 µL of AgNP-DT contains 4.9 µg of nanocatalyst. Aqueous solution of MO has an absorption maximum at 464 nm. This reduction reaction could be monitored by decrease in the intensity of peak at 464 nm and simultaneous increase in the absorbance at 250 nm (Fig. 4a). With the addition of AgNP-DT, the azo (–N=N–) bond in MO dye was reduced to corresponding colourless amine (–NH–NH–).The orange colour of the dye disappear within 10 min of time. This colour change indicates complete conversion of the dye to its corresponding amine compound.

The reduction process was also monitored by carrying out FTIR analysis of the dye solution before and after the addition of $NaBH_4$ and AgNP-DT (Fig. 3). Methyl orange display a peak at 2920 cm^{-1} for asymmetric $–CH_3$ stretching vibrations, peaks at 1676 cm^{-1} and 1646 cm^{-1} represents –C–H bending of aromatic rings. Peaks at 1031 cm^{-1}, 939 cm^{-1} and 690 cm^{-1} for –C–H stretching vibrations of benzene ring and a peak at 817 cm^{-1} for –C–H stretching vibrations in di-substituted benzene ring [47]; this confirms aromatic nature of dye. Peaks at 1600 cm^{-1} and 1516 cm^{-1} for –N=N– stretching vibrations [47] and peaks at 1361 cm^{-1} and 1184 cm^{-1} for –C–N stretching confirm the azo nature of dye [48]. The peak at 1111 cm^{-1} corresponding to –S=O stretching vibrations confirm the sulfonic nature of the MO [48]. The FTIR spectra of the reduced product of MO after the addition of $NaBH_4$ and AgNP-DT display an intense broad distinct peak at 3290 cm^{-1} for –N–H stretching of amine and peak at 1653 cm^{-1} for –N–H bending vibrations; this confirms the reduction of azo group to amine.

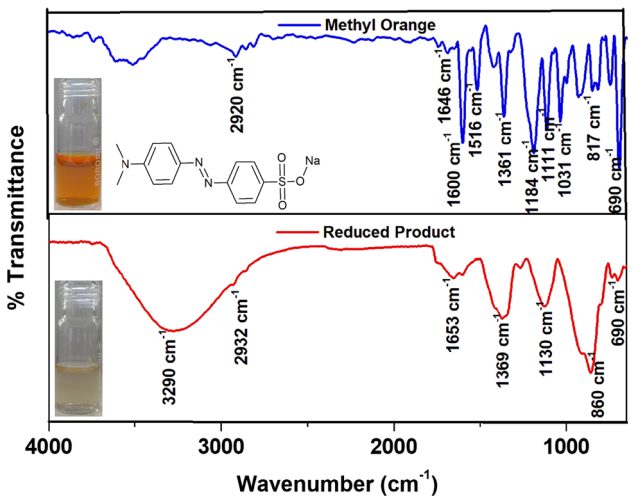

Fig. 3 FTIR spectrum of methyl orange and reduced product of methyl orange

Also, missing of peaks at 1600 cm^{-1} and 1516 cm^{-1} for –N=N– stretching vibrations further confirm the reduction of the azo group. The peak at 2932 cm^{-1} represents asymmetric $–CH_3$ stretching vibrations and peak at 1369 cm^{-1} for –C–N stretching vibrations. The peak at 1128 cm^{-1} corresponding to –S=O stretching vibrations confirm the presence of sulfonic group in the reduced product. Peaks at 904 cm^{-1}, 860 cm^{-1} and 690 cm^{-1} represents –C–H stretching vibrations of benzene ring. FTIR spectrum of the reduced product have displayed different peaks compared to the initial solution of MO, which confirms that MO has been reduced.

In the above reaction process, the concentration of $NaBH_4$, is much higher than that of MO and therefore almost remains constant throughout the reaction. Therefore, first order kinetics was applied to calculate the catalytic performance of AgNP-DT. The rate constant (k) was calculated from the linear plot of ln (A) versus reduction time (t) in minutes. The correlation coefficient for the plot was found to be $R^2 = 0.9944$. The pseudo-first order rate constant (k) and activity parameter for MO degradation for the present study were found to be 0.3208 min^{-1} and 1086 s^{-1} g^{-1} respectively (Fig. 4b). It is more appropriate to define the activity parameter of a catalytic reaction for comparing the efficiency of catalyst than merely comparing the rate constants. The activity parameter denotes the rate constant of a reaction per gram of the catalyst used [49]. The high activity parameter observed for our catalyst may be due to the higher surface area provided by AgNP-DT for the adsorption of MO and BH_4^-, which increases the rate of reduction reaction by increasing the electron transfer between these molecules. Furthermore, the effect of catalyst loading on the rate of reaction was studied by adding 8 µg of AgNP-DT, while keeping other parameters constant. The newly observed rate constant and activity parameter for the reaction were found to be 0.7221 min^{-1} and 1461 $s^{-1}g^{-1}$ respectively. Therefore it can be concluded that the rate of reaction as well as activity parameter increases with increase in the catalyst loading, which is evident due to increase in the effective catalytic surface area for the reduction reaction. Thus the high catalytic activity of our catalyst can be explained on the basis of its small size and large surface area. Above results show that AgNP-DT synthesized using the seed extract of *Derris trifoliata* can be used as a promising catalyst for the reduction reaction of water soluble dyes and effluents.

Spectrophotometric Detection of Hg^{2+} in the Aqueous Solution Using AgNP-DT

Selectivity and Sensitivity for Mercury(II) Ion Detection

The as-prepared AgNP-DT was tested for the selective detection of metal ions from aqueous solution. To

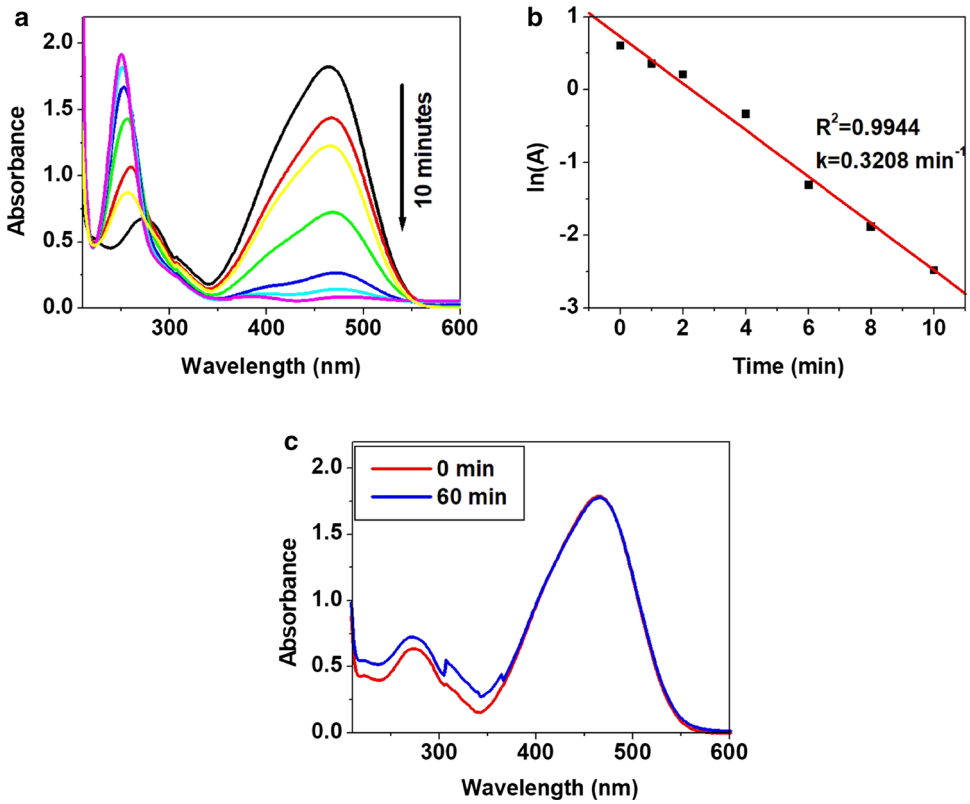

Fig. 4 **a** Reductive degradation of methyl orange in presence of 30 μL of AgNP-DT, **b** pseudo first order kinetic plot of ln (A) against time and **c** uncatalysed reduction of methyl orange

investigate the response of AgNP-DT to metal ions, 500 μL of 10^{-4} M solution of 14 different metal ions were added separately to the former solution at room temperature. It was observed that within 2 min of addition, the characteristic yellow colour of AgNP-DT got decolourised after mercury addition There was no decolourisation with metals other than mercury (Fig. 5a). This property of AgNP-DT could be utilized for the detection of Hg^{2+} ions selectively in water samples even with our naked eye. Gradual colour change of AgNP-DT with increasing concentration of Hg^{2+} is shown in (Fig. 5b). The limit of detection in case of visual detection method is 56 μM.

To investigate the sensitivity of the method, UV–Vis titration studies were done with AgNP-DT versus different concentrations of Hg^{2+}. The interaction between AgNP-DT and Hg^{2+} ions was clear from the drastic change in the intensity of SPR peak as confirmed from UV–Vis spectroscopic studies. The absorbance of SPR peak decreased and blue shifted with increasing concentration of Hg^{2+} (Fig. 4b). A linear graph ($y = -0.00353x + 0.23982$) was obtained by plotting absorbance against concentration of Hg^{2+} (Fig. 6c). From the data obtained, the limit of detection (LOD) and limit of quantification (LOQ) for the colorimetric detection of Hg^{2+} was found to be 1.55 μM and 4.7 μM respectively.

Mechanism of Sensing Activity of AgNP-DT Towards Hg^{2+}

To elucidate the mechanism of sensing activity of AgNP-DT towards Hg^{2+}, the nanoparticles were examined before and after the addition of Hg^{2+} using DLS measurements. Variation of zeta potential of AgNP-DT with increasing concentration of Hg^{2+} was also monitored. When a drop of Hg^{2+} was added to AgNP-DT aqueous solution, the stability of bio-stabilised silver nanoparticles decreases, which could be confirmed from zeta potential measurements. The average size of nanoparticles also increases with the addition of Hg^{2+} ions (Fig. 6). On further increasing the concentration of Hg^{2+}, zeta potential again decreases destabilising the nanoparticle.

This is explained as follows: Biological ligands stabilising the AgNP-DT could efficiently reduce Hg^{2+} to form Hg^{0}. This reaction weakens the electrostatic binding between biological ligands and silver nanoparticles leading to destabilisation of AgNP-DT. The as-generated mercury atoms could quickly undergo a redox reaction with zero-valent silver having a standard potential of 0.8 V (Ag^{+}/Ag) and 0.85 V (Hg^{2+}/Hg) respectively thereby forming an amalgam between Ag and Hg [50, 51]. In order to attain stability, these weakly stabilised amalgamated silver nanoparticles aggregates to form large particles, resulting in a quenching of SPR peak intensity [52]. From DLS measurements, the average size of the nanoparticle

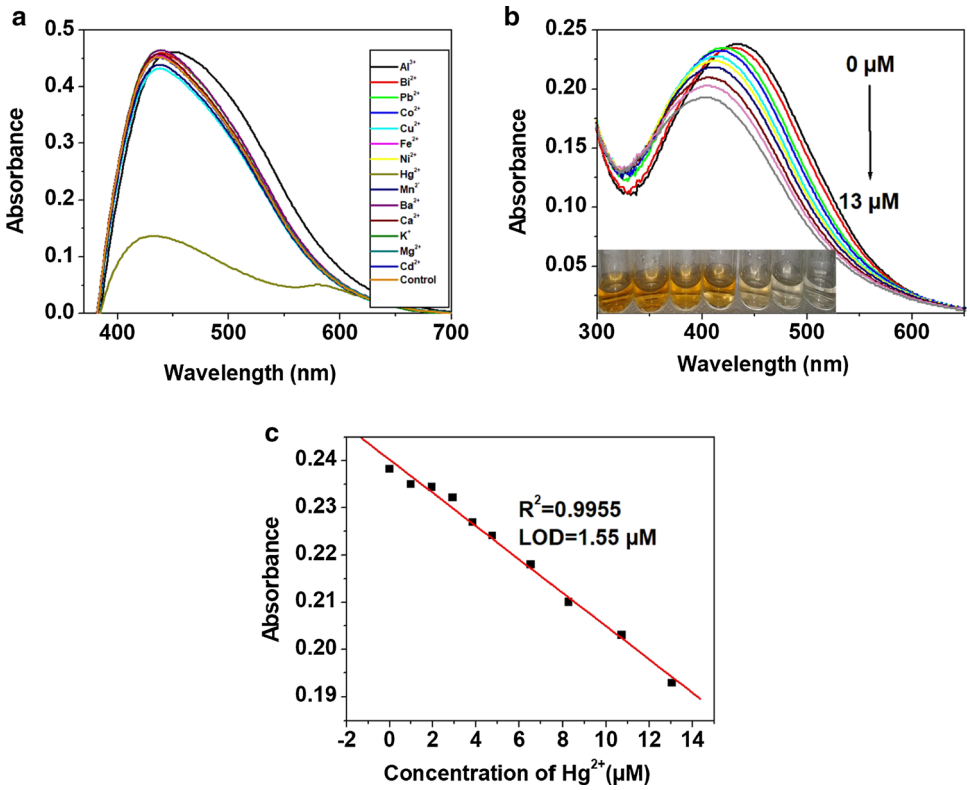

Fig. 5 **a** Selective sensing of Hg^{2+} by AgNP-DT over other metal ions, **b** sensitivity of AgNP-DT towards varying concentration of Hg^{2+}; Inset (**b**) shows the visual detection limit for the titration of AgNP-DT versus different concentrations of Hg^{2+} and **c** linear relationship of absorbance with concentration of Hg^{2+}

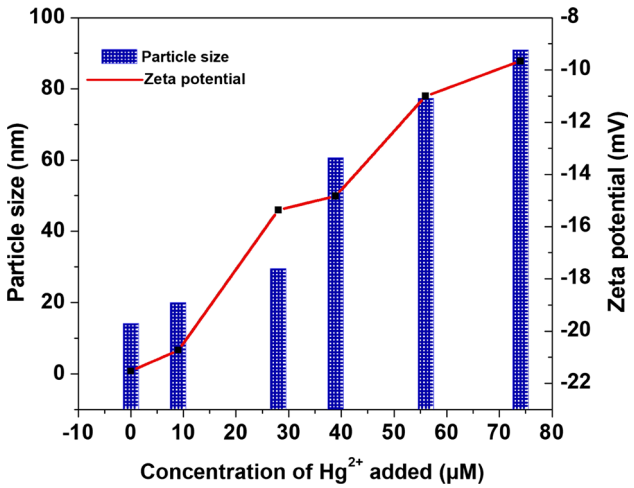

Fig. 6 Variation of zeta potential and average particle size of nanoparticle with increasing concentration of Hg^{2+}

increases to 90 nm with the addition of 80 μM of Hg^{2+}. The blue shift observed in the SPR band might be due to the above redox reaction between zero-valent silver and Hg^{2+}.

Determination of Hg^{2+} in Real Water Matrix

The proposed method was evaluated for determining Hg^{2+} in river tap water matrix. Water samples were collected from Meenachil River, Kerala, India and tap water was collected from School of Environmental Sciences, MG University campus. Both water samples were free of mercury ions. So the collected real water samples were spiked with a various concentration range of mercury and analysed according to the proposed method. The recoveries of Hg^{2+} in real water samples were measured [53], which are in range of 91.41%–108.07% (Table 1). Hence our proposed method has a great potential for the colorimetric sensing of Hg^{2+} ions in real water samples.

Table 1 Analytical results of Hg^{2+} in river water and tap water samples (n = 3)

Sample	Hg^{2+} (μM) added	Hg^{2+} (μM) found	% Recovery
River water	0	–	–
	6.54	5.99	91.56
	10.71	9.79	91.41
	19.35	17.94	92.76
Tap water	0	–	–
	6.54	7.07	108.07
	10.71	10.92	101.96
	19.35	18.70	96.64

Conclusions

In this report, stable AgNP-DT was prepared using $AgNO_3$ as the precursor and aqueous seed extract of *Derris trifoliata* as reducing and stabilising agent. From the FTIR spectral data, carbonyl and amine groups of the extract were mainly involved in the reduction and stabilization of silver nanoparticles. The as-prepared nanoparticles characterised by various spectroscopic and microscopic techniques revealed the spherical crystalline nature of AgNP-DT with an average particle size of 16.05 ± 5.0 nm. 30 μL (4.9 μg) of AgNP-DT could effectively reduce methyl orange in the presence of $NaBH_4$ with an exceptional rate constant of 0.3208 min^{-1}. Furthermore, AgNP-DT could selectively detect Hg^{2+} ions from aqueous solution. With increasing amount of Hg^{2+}, the intensity of yellow colour of AgNP-DT decreases and finally got colourless. As a result, the absorbance of AgNP-DT was decreased, which was attributed to the amalgam formation between Ag and Hg. Moreover this simple and fast method was applied to monitor the concentration of Hg^{2+} in a real water matrix.

Acknowledgements The author (NC) is grateful to University Grants Commission (UGC), Government of India, New Delhi, India for providing financial assistance under the Faculty Development Programme. The authors are thankful to Inter-University Instrumentation Centre (DST-SAIF and DST-PURSE, Govt. of India) and School of Environmental Sciences, MGU (KSCSTE-SARD, VERC Project, Govt. of Kerala) for providing the instrumentation facility as well as other support. The authors are also thankful to Dr. A.P. Thomas, Director, ACESSD and Dr. C.T. Aravindakumar, Professor, SES-MGU for their valuable support for the study.

Compliance with Ethical Standards

Conflicts of interest The authors declare that they have no conflict of interest.

References

1. G. Mance *Pollution Threat of Heavy Metals in Aquatic Environments* (Springer, Berlin, 2012).
2. K. Naseem, Z. H. Farooqi, R. Begum, and A. Irfan (2018). *J. Clean. Prod.* **187**, 296.
3. M. Saeed, A. Ahmad, R. Boddula, Inamuddin, Au Haq, and A. Azhar (2018). *Environ. Chem. Lett.* **16**, 287.
4. C. Nie, P. Sun, L. Zhu, S. Gao, H. Wu, and B. Wang (2017). *Environ Chem.* **14**, 188.
5. C. Fersi, L. Gzara, and M. Dhahbi (2005). *Desalination* **185**, 399.
6. D. Mani and C. Kumar (2014). *Int. J. Environ. Sci. Technol.* **11**, 843.
7. C. Liu, P. Wu, L. Tran, N. Zhu, and Z. Dang (2018). *Environ. Chem.* **15**, 286.
8. L. M. Soldatkina and E. V. Sagaidak (2010). *J. Water Chem. Technol.* **32**, 212.
9. S. S. Hassan, A. R. Solangi, M. H. Agheem, Y. Junejo, N. H. Kalwar, and Z. A. Taga (2011). *J. Hazard. Mater.* **190**, 1030.
10. H. Hu, J. H. Xin, H. Hu, X. Wang, D. Miao, and Y. Liu (2015). *J. Mater. Chem. A* **3**, 11157.
11. Y.-C. Chang and D.-H. Chen (2009). *J. Hazard. Mater.* **165**, 664.
12. P. Wang, B. Huang, X. Qin, X. Zhang, Y. Dai, J. Wei, and M. H. Whangbo (2008). *Angewandte Chemie Int. Edn.* **47**, 7931.
13. S.-Y. Lin, Y.-T. Tsai, C.-C. Chen, C.-M. Lin, and C.-H. Chen (2004). *J. Phys. Chem. B* **108**, 2134.
14. N. Kulkarni and U. Muddapur (2014). *J. Nanotechnol.* **2014**, 510246.
15. P. Kumar, M. Govindaraju, S. Senthamilselvi, and K. Premkumar (2013). *Colloids Surf B Biointerfaces* **103**, 658.
16. Q. Wang, D. Kim, D. D. Dionysiou, G. A. Sorial, and D. Timberlake (2004). *Environ. Pollut.* **131**, 323.
17. M. C. Houston (2011). *J. Clin. Hypertens.* **13**, 621.
18. K. Leopold, M. Foulkes, and P. Worsfold (2010). *Analytica Chimica Acta.* **663**, 127.
19. S. W. Thomas, G. D. Joly, and T. M. Swager (2007). *Chem. Rev.* **107**, 1339.
20. N. Wanichacheva, M. Siriprumpoonthum, A. Kamkaew, and K. Grudpan (2009). *Tetrahedron Lett.* **50**, 1783.
21. K. Farhadi, M. Forough, R. Molaei, S. Hajizadeh, and A. Rafipour (2012). *Sensors Actuators B Chem.* **161**, 880.
22. R. Tabaraki and N. Sadeghinejad (2018). *Ecotoxicol. Environ. Saf.* **153**, 101.
23. F. Geng, X. Jiang, Y. Wang, C. Shao, K. Wang, P. Qu, and M. Xu (2018). *Sensors Actuators B Chem.* **260**, 793.
24. X. Zhang, W. Shi, X. Chen, and Z. Xie (2018). *Sensors Actuators B Chem.* **255**, 3074.
25. H. Yu, D. Long, and W. Huang (2018). *Sensors Actuators B Chem.* **264**, 164.
26. Y. Zhou, W. Huang, and Y. He (2018). *Sensors Actuators B Chem.* **270**, 187.
27. M. Zhao, H. Yu, and Y. He (2019). *Sensors Actuators B Chem.* **283**, 329.
28. Y. Gao, K. Wu, H. Li, W. Chen, M. Fu, K. Yue, X. Zhu, and Q. Liu (2018). *Sensors Actuators B Chem.* **273**, 1635.
29. H. Liu, Y. Ding, B. Yang, Z. Liu, Q. Liu, and X. Zhang (2018). *Sensors Actuators B Chem.* **271**, 336.
30. X. Zhu, W. Chen, K. Wu, H. Li, M. Fu, Q. Liu, and X. Zhang (2018). *New J. Chem.* **42**, 1501.
31. X. Xue, F. Wang, and X. Liu (2008). *J. Am. Chem. Soc.* **130**, 3244.
32. J. Du, M. Zhao, W. Huang, Y. Deng, and Y. He (2018). *Anal. Bioanal. Chem.* **410**, 4519.
33. S. Kaviya and E. Prasad (2014). *ACS Sustain. Chem. Eng.* **2**, 699.
34. N. Bonnia, M. Kamaruddin, M. Nawawi, S. Ratim, H. Azlina, and E. Ali (2016). *Procedia Chem.* **19**, 594.
35. A. Harborne *Phytochemical Methods a Guide to Modern Techniques of Plant Analysis* (Springer, Berlin, 1998).
36. S. Ahmed, M. Ahmad, B. L. Swami, and S. Ikram (2016). *J. Adv. Res.* **7**, 17.
37. S. Francis, S. Joseph, E. P. Koshy, and B. Mathew (2017). *New J. Chem* **41**, 14288.
38. A. Patterson (1939). *Phys. Rev.* **56**, 978.
39. C. Jiang, S. Liu, W. He, X. Luo, S. Zhang, Z. Xiao, X. Qiu, and H. Yin (2012). *Molecules* **17**, 657.
40. A. Yenesew, J. T. Kiplagat, S. Derese, J. O. Midiwo, J. M. Kabaru, M. Heydenreich, and M. G. Peter (2006). *Phytochemistry* **67**, 988.
41. L.-R. Xu, J. Wu, and S. Zhang (2006). *J. Asian Nat. Prod. Res.* **8**, 9.
42. Y. Takeda, K. Yano, H. Ayabe, T. Masuda, H. Otsuka, E. Sueyoshi, T. Shinzato, and M. Aramoto (2008). *J. Nat. Med.* **62**, 476.
43. M. Nasrollahzadeh, S. M. Sajadi, E. Honarmand, and M. Maham (2015). *New J. Chem.* **39**, 4745.

44. V. Vidhu and D. Philip (2014). *Micron* **56**, 54.
45. V. Vidhu and D. Philip (2014). *Spectrochimica Acta Part A Mol. Biomol. Spectrosc.* **117**, 102.
46. D. Kang and M. Trenary (2000). *Surf. Sci.* **470**, L13.
47. D. C. Kalyani, A. A. Telke, S. P. Govindwar, and J. P. Jadhav (2009). *Water Environ. Res.* **81**, 298.
48. T. Shen, C. Jiang, C. Wang, J. Sun, X. Wang, and X. Li (2015). *RSC Adv.* **5**, 58704.
49. B. Baruah, G. J. Gabriel, M. J. Akbashev, and M. E. Booher (2013). *Langmuir* **29**, 4225.
50. T. Liu, J. X. Dong, S. G. Liu, N. Li, S. M. Lin, Y. Z. Fan, J. L. Lei, H. Q. Luo, and N. B. Li (2017). *J. Hazard. Mater.* **322**, 430.
51. K. Z. Kamali, A. Pandikumar, S. Jayabal, R. Ramaraj, H. N. Lim, B. H. Ong, C. S. D. Bien, Y. Y. Kee, and N. M. Huang (2016). *Microchimica Acta.* **183**, 369.
52. P. Vasileva, T. Alexandrova and I. Karadjova (2017). *J. Chem.* **2017**.
53. L.-J. Huang, R.-Q. Yu, and X. Chu (2015). *Analyst* **140**, 4987.